General Disclaimer

One or more of the Following Statements may affect this Document

- This document has been reproduced from the best copy furnished by the organizational source. It is being released in the interest of making available as much information as possible.

- This document may contain data, which exceeds the sheet parameters. It was furnished in this condition by the organizational source and is the best copy available.

- This document may contain tone-on-tone or color graphs, charts and/or pictures, which have been reproduced in black and white.

- This document is paginated as submitted by the original source.

- Portions of this document are not fully legible due to the historical nature of some of the material. However, it is the best reproduction available from the original submission.

NASA TECHNICAL MEMORANDUM

NASA TM-78944

NASA TM-78944

PRELIMINARY STUDY OF THE EFFECT OF THE TURBULENT FLOW FIELD AROUND COMPLEX SURFACES ON THEIR ACOUSTIC CHARACTERISTICS

by W. A. Olsen and D. Boldman
Lewis Research Center
Cleveland, Ohio

TECHNICAL PAPER to be presented at the
Eleventh Fluid and Plasma Dynamics Conference
sponsored by the American Institute of Aeronautics and Astronautics
Seattle, Washington, July 10-12, 1978

PRELIMINARY STUDY OF THE EFFECT OF THE TURBULENT FLOW FIELD AROUND COMPLEX SURFACES ON THEIR ACOUSTIC CHARACTERISTICS

by W. A Olsen and D. Boldman

National Aeronautics and Space Administration
Lewis Research Center
Cleveland, Ohio

E-9691

INTRODUCTION

The noise caused by a turbulent airstream passing over a fixed surface is of practical interest. Among the surfaces of interest are the fixed surfaces in the flow passages of an engine (e. g. stators, splitters, supports, etc.), and the wing and flaps of STOL aircraft. A number of these surfaces have been studied acoustically at the Lewis Research Center. However, the turbulent flow properties around most of these surfaces have not been measured in adequate detail

The objectives of the present study were to make fairly extensive measurements of the turbulent flow around these types of surfaces, and to use these measurements and available theory to explain their varied acoustic characteristics. This will help improve our understanding of the noise generation mechanisms and also aid in the development of future analyses.

In figure 1 are shown the configurations that were selected for this study because their acoustic characteristics are vastly different. Fundamental aeroacoustic theories exist only for a few simple configurations with simple flows (fig. 1(a)). Only approximate semi-empirical models exist for the complex flows around the complex surfaces (e. g. fig. 1(b)), but the role of turbulence in the noise generation process should be essentially the same as it is for the simple configurations. The noise generation will be due to the sum of sur-

AIAA 78-1123

face and volume sources. A fundamental theory exists (refs. 1 and 2) that predicts the complete noise emission from finite chord airfoils immersed in homogeneous one dimensional turbulent flow (figs. 1(a-2) and 1(a-3)). This surface source theory has no empirically adjusted parameters, and the analytical results are in excellent agreement with data (refs. 3 and 4). Fundamental jet noise theory (ref. 1) is in excellent agreement with data (e.g. refs. 5 and 6); however, it has some empiricism. The nonhomogeneous, nonisotropic turbulent flow around the complex surfaces makes it very difficult to relate measured turbulent flow data to the acoustic emission. Nevertheless, this task can conceivably still be accomplished for the following reasons:

(1) The fundamental theories for the simple configurations indicate that measurements of the magnitude of the mean velocity vector and the turbulence properties in the flow direction (intensity, integral scale length, and spectra) are necessary and sufficient to calculate the noise emission from the simple configurations. It is reasonable to assume that any fundamental or semi-empirical theory for complex surfaces, with their complex flows, would also be adequately described by these variables. The spatial distribution of the flow properties around the complex surfaces, is required.

(2) References 7 and 8 indicate that the measurement of the mean flow velocity and turbulence could be adequately accomplished with simple fixed-frame single-point measurements at very low velocity.

(3) The effect of turbulence on the acoustic emission can be broken down into two factors. One factor affects only the shape of the radiation pattern and the velocity power law. The other factor affects only the acoustic spectra.

Only the factor affecting the radiation pattern and the velocity power law is discussed in this paper. The radiation pattern and the velocity power law are primarily affected by the surface size and by the closeness of regions of significant turbulence to the surface edges. This point is illustrated in the appendix, where the simple configurations in figure 1(a) are discussed.

APPARATUS AND PROCEDURE

The flow from a nozzle was directed upon various two-dimensional surface configurations such as the three-flap model shown in figure 2. The model wings were supported at their ends by a rigid steel channel framework that was attached to the nozzle inlet pipe. The flow from a high pressure air supply passed through a large plenum that contained a series of screens, flow straighteners, and filters. The filters permitted operation with hot wires at velocities up to 200 meters per second.

Turbulence measurements were taken for the complex surface configurations shown in figure 1(b). The geometry and acoustic data for these configurations have been reported previously as follows. A 5.3 centimeter diameter circular nozzle was used with the three-flap (fig. 1(b-1)) and solid wing (fig. 1(b-2)) models, which are described in reference 9. The nozzle-over-the-wing (OTW) configuration (fig. 1(b-3)), described in reference 10, employed a slot nozzle (equiv. diam 5.3 cm) with side doors. Other turbulence tests involved the circular nozzle alone (fig. 1(a-1)) as a check with published data. Turbulence results for a small chord airfoil (fig. 1(a-2)) and a large plate (fig. 1(a-4)) were published earlier in references 3 and 11, respectively.

Nozzle exit velocities, V_n, were determined from measurements of the pressure and temperature of the air in the plenum. Most of the tests were conducted with an exit velocity of 95 meters per second; however, a limited number of tests were conducted at velocities up to 200 meters per second.

Single point measurements of the mean velocity and turbulence velocities were taken with a commercially available hot wire anemometer and signal processing system. The majority of measurements were obtained with a single hot wire oriented normal to the midspan plane and traversed in that plane with a motorized actuator. Since there was no spanwise flow in the midspan plane, the hot wire was always oriented normal to the mean velocity vector. Consequently, the wire sensed the mean and turbulence velocities (U_1, u_1) in the longitudinal or streamwise direction, x_1. A tuft was used to align the wire normal to the

velocity vector at other spanwise positions. The mean velocity was plotted as a function of probe position on an x-y recorder. The hot wire position was manually referenced to the test surface to within about ±0.05 centimeter.

A 0.0005 centimeter diameter tungsten hot wire was used. The signal from the single wire probe was linearized (i.e. output potential was made a linear function of mean velocity) and monitored on a direct current voltmeter for the mean velocity vector magnitude, U_1. A true root-mean-square (rms) meter was used to monitor $\tilde{u}_1$. Signals were recorded on magnetic tape and analyzed subsequently with a narrow-band spectrum analyzer having an effective bandwidth of 6 Hz over a frequency range of 20 Hz to 50 kHz. The resulting turbulence spectra were used to determine the longitudinal integral scale length. The hot wire was calibrated prior to each test by placing it in the center of the jet near the nozzle exit. In this linearized system, nonlinear distortion of the signal was less than 5 percent of the mean velocity at velocities up to 95 meters per second.

RESULTS AND DISCUSSION

The first part of this section contains a discussion of contour plots of the longitudinal mean velocity and turbulence intensity, which are used to describe the complex flow field around the complex surfaces. In the second part, these turbulent flow field measurements and an approximate theory are used to estimate the acoustic characteristics (i.e. the shape of the radiation pattern and the velocity power law).

Turbulent Flow Field Description

Circular jet. - Limited measurements were taken in the jet from the circular nozzle (fig. 1(a-1)) in order to check the hot wire measurements against data in the literature. The mean velocity and turbulence intensity, spectra, and scale length were in close agreement with the measured results in reference 8.

Three-flap configuration. - In this configuration (ref. 9), additional lift is generated by moving a series of flaps into the jet. The turbulent flow near these flaps generates considerable additional noise. Contour plots of the flow measurements for this configuration are shown on figure 3. Constant-value contours of the ratio of the local velocity to the nozzle exhaust velocity, U_l/V_n, are shown on figure 3(a). Turbulence intensity, $\tilde{u}_l/V_n$, contours are shown on figure 3(b). The contours were determined by interpolation of data obtained from midspan hot wire traverses along the lines numbered 0 to 12 on figure 3. The regions of highest turbulence intensity occur near the last flap. The maximum turbulence intensity (16 percent) occurs above the trailing edge of the last flap; below this region there is a less intense region (12 percent). The maximum turbulence intensity for the jet is 14 percent. The impact region of the jet flow on the three-flap wing contains no intense turbulence.

The solid dots in figure 3, and others following, denote the locations where longitudinal turbulence spectra were measured. The measurements, in turn, were used to determine the longitudinal integral scale lengths, ℓ_l, which appear in the boxes on the figures. This scale length is used in the surface source equations which are discussed later.

Slotless wing. - In this configuration a simply curved plate is used to deflect the jet from the 5.2 centimeter diameter nozzle (ref. 9). Mean velocity and turbulence intensity contours are plotted on figures 4(a) and (b), respectively. The flow is similar to that of the three-flap configuration in that the flow from the nozzle is essentially undisturbed until it is fairly close to the surface. Furthermore, there are two regions of maximum turbulence intensity (16 percent) downstream of the trailing edge. There are two points of difference: the flow is much less complex, and the impact region of the jet, which is located far from the edge of the surface, has a region of high turbulence intensity (16 percent).

OTW configuration. - This configuration uses a slot-like nozzle over a solid wing (ref. 10). The nozzle has partially open side doors for better flow attachment. Figures 5(a) and (b) contain the velocity and intensity contours in the midspan plane. The flow field downstream

of the wing is similar to that of the slotless wing in that there are two regions of peak intensity downstream of the trailing edge. However, the maximum intensity for this configuration (18 percent) is quite high compared with that for the previous configurations. Furthermore, it occurs over a large region of the flow.

Traverses were also made for several spanwise locations at station no. 4 (see fig. 5). The hot wire was oriented normal to the flow to account for the small spanwise flow component. Contour plots of the data are shown on figures 6(a) and (b). The two regions of peak intensity shown on figure 5 extend spanwise about 1-1/2 nozzle half-widths to each side of the midspan plane.

Estimate of the Acoustic Characteristics

Formulation of equations. - In order to account for the complex inhomogeneous turbulent flow around the complex surfaces, some approximate theoretical equations of references 1 and 12 are adapted for use herein. The resulting equations describe the peak of the noise spectrum caused by a small volume of turbulent flow very near to (surface source) and very far from (volume source) the edge of an infinite plate. The approximate order of magnitude analysis, used in references 1 and 12 to evaluate the turbulence tensors in the theory, were modified slightly for this work. The resulting equations are consistent with the results from the fundamental theories and experiments for airfoil (surface source) and jet noise (volume source). These equations will be used to qualitatively relate measurements of the turbulent flow around the complex surfaces to the measured acoustic characteristics.

The effect of geometry and the turbulent flow distribution on the acoustic emission from the simple configurations in figure 1(a) are discussed in the appendix. Table I contains a summary of the measured acoustic characteristics and indicates how well the theory predicts them. The measured acoustic characteristics for the complex configurations are also summarized in table I. The reader may find these helpful in understanding the physical ideas used in the formulation that follows.

To obtain the noise from the complex surfaces, the turbulent flow is divided into a number of small but finite volume elements. For each element, it is assumed that the turbulence is homogeneous and isotropic, and the mean flow is one-dimensional. Each element is characterized by the local flow properties and its turbulent flow is the cause of volume and surface noise sources that are assumed to be acoustically independent. The total far field noise is the result of the sum of the intensities from the volume and surfaces sources throughout the flow field. Surface sources occur where there is significant turbulence near the edge of a surface. Volume sources are always present; but surface sources are more efficient emitters, therefore they often dominate the volume sources at low velocity.

Volume sources. - The peak of the acoustic intensity spectrum caused by an elemental volume source would be described by

$$I_{pv} \propto \underbrace{\left[\frac{(\tilde{u}_1)^8}{R^2 \ell_1^1}\right]}_{\text{Amplitude}} \underbrace{\left(1 - 0.62 \frac{V_n}{C_o} \cos \theta_e\right)^{-3}}_{\text{Radiation pattern}} \tag{1}$$

The amplitude of this equation is taken directly from reference 1 (Chapter 3). The radiation pattern is taken from Chapter 6; it is applicable to jet noise and the noise from an infinite plate (see table I).

To be consistent with the data on figures 3 to 6 the amplitude in equation (1) is rearranged to include the nozzle velocity, V_n.

$$I_{pv} \propto \underbrace{\underbrace{\frac{V_n^8}{R^2}\underbrace{\left(\frac{\tilde{u}_1}{V_n}\right)^8 \frac{1}{\ell_1^1}}_{\text{Local flow properties}}}_{\text{Amplitude at } \theta_e = 90^o}}_{\text{Amplitude at } \theta_e = 90^o} \underbrace{\left(1 - 0.62 \frac{V_n}{C_o} \cos \theta_e\right)^{-3}}_{\text{Radiation pattern}} \tag{2}$$

This equation, and those that follow for surface noise, involve two factors: the amplitude at $\theta_e = 90^o$, and the shape of the radiation pattern. The angle where I_{pv} is maximum will occur near the flow exhaust (i.e. $\theta_e \rightarrow 0^o$). The amplitude is dependent on the nozzle velocity to some power and the local flow properties. Equation (2) indicates that the strongest volume sources occur wherever $\tilde{u}_1/V_n$ is largest. The effect on the amplitude of changes in the correlation length for the volume source, ℓ_1^1, is very small. (However, the effect on the acoustic spectra, not discussed herein, is not small.) The correlation length can be determined from the single wire data as indicated in the nomenclature. This length is different from the integral scale length, ℓ_1, which is used in the subsequent surface source equations.

The far field noise due to the volume sources is calculated by summing the I_{pv} from each volume element. The summation is made at each θ_e. The typical equation for subsonic jet noise, involving the nozzle area, will result from equation (2) by summing I_{pv} for each volume element of the jet (fig. 1(a-1)) and accounting for the turbulent flow distribution. This equation has also been used in reference 11 to account for the volume source noise from an infinite plate (fig. 1(a-4)). Experiments reported in reference 15 have shown that the radiation pattern from an infinite plate is approximately described by equation (2), provided the impingement angle of the jet is less than 60^o.

Surface sources. - The intensity of the acoustic spectrum peak from the surface source falls between the bounds defined by the equations given next, depending on the ratio of the chord length of the surface to longitudinal turbulence scale length, C/ℓ_1.

(1) For very large chord airfoil ($C/\ell_1 > 10$, see fig. 1(a-3)) the source (fluctuating lift) is concentrated within a few scale lengths of the edge. One of two equations is used to describe this case; the choice depends on which edge has the dominant turbulent source.

(a) If the amplitude of the turbulence source at the leading edge is at least equal to that at the trailing edge, then the leading edge is the dominant source, and

$$I_{ps} \propto \frac{U_1^5}{R^2}\left(\frac{\tilde{u}_1}{U_1}\right)^2 \frac{1}{\ell_1}\left(\frac{r_o}{\ell_1}\right)^{-3} \cos^2\left(\frac{\theta_e}{2}\right)$$

$$= \underbrace{\frac{V_n^5}{R^2}\underbrace{\left(\frac{U_1}{V_n}\right)^3\left(\frac{\tilde{u}_1}{V_n}\right)^2 \frac{1}{\ell_1}\left(\frac{r_o}{\ell_1}\right)^{-3}}_{\text{Local flow properties}}}_{\text{Amplitude}} \underbrace{\cos^2\left(\frac{\theta_e}{2}\right)}_{\text{Radiation pattern}} \qquad (3a)$$

the maximum value[1] of I_{ps} occurs at $\theta_e = 0^o$.

(b) If the leading edge turbulence source amplitude is much less than that at the trailing edge, then the trailing edge source dominates and the radiation pattern term changes

$$I_{ps} \propto \frac{V_n^5}{R^2}\left(\frac{r_1}{V_n}\right)^3\left(\frac{\tilde{u}_1}{V_n}\right)^2 \frac{1}{\ell_1}\left(\frac{r_o}{\ell_1}\right)^{-3} \sin^2\left(\frac{\theta_e}{2}\right) \qquad (3b)$$

Equation (3b) indicates that the maximum[1] value of I_{ps} occurs at $\theta_e = 180^o$.

Equations (3a) and (3b) came from reference 12 by assuming that the frequency of the turbulent oscillations was proporational to U_1/ℓ_1.

(2) For very small chord airfoils, ($C/\ell_1 \ll 1$; see fig. 1(a-2)) the peak intensity would be given by

---

[1]In both cases the maximum occurs in the infinite direction of the plate.

$$I_{ps} \propto \frac{U_1^6}{R^2}\left(\frac{\tilde{u}_1}{U_1}\right)^2 \frac{1}{\ell_1}\left(\frac{r_o}{\ell_1}\right)^{-3} \sin^2\theta_e$$

$$= \frac{V_n^6}{R^2}\underbrace{\left(\frac{U_1}{V_n}\right)^4\left(\frac{\tilde{u}_1}{V_n}\right)^2 \frac{1}{\ell_1}\left(\frac{r_o}{\ell_1}\right)^{-3}}_{\text{Local flow properties}} \underbrace{\sin^2\theta_e}_{\text{Radiation pattern}} \qquad (4)$$

The maximum value of I_{ps} occurs at $\theta_e = 90^o$. In this case, where $C/\ell_1 < 1$, the source (fluctuating lift) is over the whole airfoil.

Unlike the large chord airfoil, there is no specific theory for a small chord airfoil immersed in a nonhomogeneous turbulent flow. Equation (4) is constructed by heuristic argument so that it is consistent with equation (3a) and also with the equations derived in references 1 and 2 for homogeneous turbulent flow over small-to-large chord airfoils. For homogeneous turbulence, equations (3a) and (4) transform to the equations listed in table I, which include the scrubbed area of the airfoil (bC).

Experimental results (ref. 3) indicate that airfoils with intermediate chord lengths ($1 < C/\ell_1 < 10$) will have velocity power laws and radiation patterns that fall between the limits described by equations (3) and (4).

Equations (3a), (3b), and (4) involve two factors: the widely varying radiation pattern shape, which has already been discussed, and the amplitude at $\theta_e = 90^o$. The amplitude is a strong function of the local velocity and the turbulence intensity. The surface source equations all contain the factor $(r_o/\ell_1)^{-3}$, where r_o is the distance between the edge of a surface and a point in the flow. The large negative exponent means that only the intense turbulent flow near the edge of the surface can cause the fluctuating lift on the surface that generates significant surface noise.

The amplitude is only a weak function of the longitudinal integral scale length, ℓ_1. This length is determined from single wire measure-

ments of the turbulence spectra as indicated in the nomenclature. The transverse scale length should really be used in the previous equations. However, it is more difficult to measure in a complex flow, and the amplitude is not sensitive to the scale length under any conditions. Also, the longitudinal length was measured in the center of the shear layer (i.e., maximum turbulence intensity) where the transverse length, which is constant across the shear layer, would be close to one-third of the longitudinal length.

Equations (2) and (4) describe the experimental results for the simple configurations (fig. 1(a)) very well (see table I) when the flow distribution is taken into account. However, these equations will be far less accurate when applied to the complex surfaces (fig. 1(b)) for the following reasons. First, some important acoustic effects are not included that affect the radiation pattern. These are surface reflections and shielding, refraction and other effects of a finite flow. Second, the $(r_o/\ell_1)^{-3}$ relationship has not been verified experimentally. And last, these equations can only predict the peak of the acoustic spectrum, and only in the midspan plane.

Source estimate. - The next task is to estimate from these equations, the location and strength of volume and surface sources for the complex geometries. This is accomplished by using the turbulent flow contours (plotted on figs. 3 to 5), in conjunction with the volume source equation (eq. (2)) and the appropriate equation for the surface source (either eqs. (3a), (3b), or (4)). Contour curves of constant I_{pv} and I_{ps} have been determined from these calculations. The volume source results for each configuration are shown on figure 7 by the solid contour curves. These contours were calculated from equation (2) as the ratio of I_{pv} to the maximum value among all the data. For example, the -5 and -10 decibels contours are referenced to the highest value of I_{pv} found for all configurations; the highest value (0 dB) is denoted by the solid decibel contour for the OTW configuration. The relative area of these contours is a measure of the relative strength of the volume sources for each configuration, provided the spanwise extent of these contours is the same. The OTW configuration obviously has the

strongest volume sources, whereas the three-flap configuration has the weakest.

The same type of contours were also calculated for the more intense surface sources by using the appropriate equation from equations (3a), (3b), or (4). In the calculations $(r_o\ \ell_1)^{-3}$ was set equal to unity when $r_o/\ell_1 < 1$. The theory used herein is too inexact to permit comparison of the relative strength of the surface sources for each configuration. However, the acoustic results from the varied chord experiments of reference 3 can be used to estimate the relative value of I_{ps} for the complex geometries. The value of I_{ps} would be about the same for the range of values of C/ℓ_1 and V_n that occurred in the acoustic experiments with the complex surfaces. Therefore, a qualitative comparison of the relative surface source strengths can be made for each configuration by calculating the I_{ps} contours relative to the maximum value (0 dB) for each configuration.

It is also desirable to make a relative comparison of the surface and volume source strengths. The local flow properties $\left(U_1\ V_n,\ \tilde{u}_1/V_n,\ \theta_e,\ \ell_1 \text{ and } \ell_1^1\right)$ in equations (2) to (4) are essentially independent of velocity, therefore the source strength can be estimated from the low velocity data on figures 3 to 5. But the magnitudes of I_{pv} and I_{ps} depend on different powers of the velocity $\left(V_n^5 \text{ to } V_n^8\right)$. Furthermore, equations (2) to (4) are too inexact and the spanwise measurements are insufficient for an accurate comparison. Therefore the far field acoustic results for the complex surfaces (refs. 9 and 10) must be used. These indicate that I_{ps} and I_{pv} are approximately equal at $V_n = 200$ m/s. This suggests that the surface and volume source strengths (area enclosed by a contour curve on fig. 7) can be roughly compared at $V_n = 200$ m/s. This source strength estimate, coupled with the appropriate radiation pattern, permits the following qualitative estimate of the far field noise characteristics to be made for each surface shown on figure 7.

Three-flap configuration. - The equation used to describe the surface source (from eqs. (3a), (3b), or (4)) depends upon the value of C/ℓ_1 and the location of the intense turbulence. The three-flap con-

figuration (fig. 7(a)) has a group of small airfoils that are totally immersed in the turbulent flow; therefore, equation (4) was used.[2] The contours indicate that the surface source for the three-flap configuration is concentrated near the last flap. The surface sources are of about the same strength for each complex configuration studied herein. The volume sources for this configuration are the weakest relative to the other configurations. Therefore, at the low velocity of 200 m/sec the surface sources probably dominate for the three-flap configuration, and the acoustic intensity should follow U_1^6 at all angles. The volume source, minus the effect of refraction, would nevertheless add to the noise near $\theta_e = 0^o$, especially at high velocities. This qualitative estimate is consistent with the acoustic data for this configuration (see table I).

Slotless wing. - For the slotless wing (fig. 7(b)) there is no turbulent flow at the leading edge and $C/\ell_1 > 10$, therefore equation (3b) was used. The slotless wing has its surface source concentrated at the trailing edge, therefore the maximum value for its radiation pattern should be near $\theta_e = 180^o$ where the noise should nearly follow U_1^5. The most intense volume source regions are the jet impact region and the flap exhaust region. Because of reflections off the wing and refraction the radiation pattern from these volume sources will tend to have its maximum near the flap exhaust (i.e. small θ_e). Therefore, the velocity power law will be near U_1^5 at large θ_e; this will gradually change to U_1^6 at small θ_e. This qualitative estimate is consistent with the acoustic data (see table I).

OTW configuration. - The OTW configuration (fig. 7(c)) has intense turbulence at the trailing edge and a large chord ($C/\ell_1 > 10$), therefore it is described by the same equations as used for the slotless wing. The results are also similar, except that the volume

---

[2]The chord of the last flap ($C/\ell_1 = 4$) is larger than the small chord airfoil upper limit ($C/\ell_1 < 1$), therefore the source would be closer to the leading edge and the maximum value of the radiation pattern would occur at $\theta_e \simeq 50^o$, rather than at $\theta_e = 90^o$ for the small chord airfoil.

sources are more intense because of the larger values of $\tilde{u}_1/V_n$. The larger size of the volume source region implies that the acoustic intensity will probably follow V_n^8 over a larger range of θ_e than for the slotless wing. Again, this estimate is in good agreement with the acoustic data (table I).

Figure 7(c) (and also figs. 7(a) and (b)) indicate that there are large overlapping regions of surface and volume sources that significantly contribute to the total noise (i.e. within the -10 dB contours). This overlap was also apparent in the cross correlation measurements (hot wire to far field microphone) taken in references 4, 13, and 14.

CONCLUDING REMARKS

The equations developed herein are based upon fundamental theories for simple configurations having simple flows. They have been used to qualitatively estimate the acoustic characteristics of the surfaces (i.e. radiation pattern and velocity power law from the complex spatial distribution of the turbulent flow properties around a number of complex surfaces. These estimates are consistent with the acoustic data.

This approach is helpful in improving our understanding of the complex noise generation mechanisms. However, in their present form the equations are inadequate for any qualitative estimate of the noise emission.

SYMBOLS

b	effective span of airfoil, m
C	longitudinal length of surface (e.g. chord of airfoil), m
c_o	ambient speed of sound, m/s
d	diameter of nozzle, m
$E_1\langle k_1\rangle$	one dimensional energy spectrum function for longitudinal turbulence velocity; $E_1\langle k_1\rangle\, dk_1$ is contribution to $(\tilde{u}_1)^2$ of wave numbers between k_1 and k_1 + bandwidth, m^3/sec^2

E_{1p}	value at peak of $E_1(k_1)$ spectrum, m^3/sec^2
I_p	peak of the 1/3 octave acoustic intensity spectrum per unit volume, w/m^5
I_{pv}, I_{ps}	I_p for volume source and surface sources, w/m^5
ℓ_1	longitudinal integral scale length used in the surface source equations. This two wire measurement is closely approximated (ref. 8) from fixed-frame single-wire turbulence spectral data according to $\ell_1 \approx \pi/2\ E_{1p}/(\tilde{u}_1)^2$, m
ℓ_1^1	longitudinal correlation length used in the volume source equation (1); approximated for jet noise in reference 19 by $\ell_1^1 \approx \tilde{u}_1/(\partial U_1/\partial x_2)$, m
r_o	distance from source to edge of surface, m
R	microphone radius, m
U_1	magnitude of local mean velocity vector (i.e. longitudinal velocity), m/s
u_1	longitudinal turbulence velocity, m/sec
$\tilde{u}_1/V_n$	longitudinal turbulence intensity
V_n	nozzle exhaust velocity, m/sec
x_1	longitudinal distance in direction of local mean velocity vector, m
x_2	traverse distance normal to x_1 and x_3, m
x_3	spanwise distance from midspan plane ($x_3 = 0$), m
θ_e	angle from local mean velocity vector to microphone, deg.

APPENDIX - EFFECT OF GEOMETRY AND TURBULENT FLOW DISTRIBUTION ON THE ACOUSTIC CHARACTERISTICS OF THE SIMPLE CONFIGURATIONS

Longitudinal variations in the turbulent flow distribution around a surface, and changes in the geometry of the surface, can have a profound effect on the characteristics of the acoustic emission. To illustrate this point, consider the simple configurations shown in figure 1(a). The measured acoustic emission from these configurations is described in table I.

Consider the airfoils shown on figure 1(a-1) and 1(a-2) immersed in a turbulent one dimensional mean flow; the flow is homogeneous (i. e. uniform turbulence properties) everywhere near the airfoils. The theory (refs. 1 and 2) indicates that changes in the airfoil chord causes changes in the noise source location, velocity power law, radiation pattern, and also in the spectral shape, even though the turbulence properties in the source region do not change. The velocity power law changes gradually from U_1^6 for a very small chord airfoil (fig. 1(a-2)) to U_1^5 for a very large chord airfoil (fig. 1(a-3)). The shape of the radiation pattern also gradually changes from $\sin^2\theta_e$ for the small chord to $\cos^2(\theta_e/2)$ for the very large chord; the maximum acoustic intensity is at $\theta_e = 90^o$ for the former and at $\theta_e = 0^o$ for the latter. As the chord increases, the low frequency part of the acoustic spectra at $\theta_e = 90^o$ moves to lower frequency, the high frequency part stays in place, and the spectra start to exhibit ripples. Regardless of the chord, the noise source is due to fluctuating lift caused by turbulence acting over a small region, within a few longitudinal turbulence integral scale lengths, ℓ_1, of the leading edge (see fig. 1(a-3)).

Experimental results for airfoils of various chords, which were immersed in homogeneous and nonhomogeneous turbulent flow, are reported in references 3 and 4. These results indicate that the homogeneous flow theory for the small chord airfoil accurately describes the spectra and the shape of the radiation pattern that was measured for

small chord airfoils ($C/\ell_1 < 1$). The whole airfoil acts as the source. These data also indicate that the homogeneous theory for the infinite chord airfoil adequately predicts the radiation pattern and spectra for airfoils whose chord is larger than 10 scale lengths, $C/\ell_1 > 10$.

If the turbulence at the leading edge is much less than that at the trailing edge (e.g. figs. 1(b-2) and 1(b-3)), then the source would be at the trailing edge. The radiation pattern, predicted by the homogeneous theory for an infinite chord airfoil with the source at the trailing edge, would be a mirror image of the leading pattern (i.e. $\sin^2(\theta_e/2)$) with its maximum still in the infinite plate direction.

The effects of a nonhomogeneous finite jet (e.g. refraction, fluid shielding, etc.) will modify the radiation patterns predicted above from the homogeneous flow theories. The analysis in reference 18 and the data in reference 3, the airfoils immersed in a finite jet, indicate the following differences from the results of homogeneous flow theory. The homogeneous pattern for the small chord airfoil is only slightly in error at high and low frequency wherever $\theta_e < 60^o$. The homogeneous leading edge pattern is accurate except for low frequency when the velocity is high. The homogeneous trailing edge pattern is only correct at low velocity; in fact, at high velocity the homogeneous leading edge pattern is more nearly correct.

Suppose there is no significant turbulence near any edge. Examples of this would be an isolated jet (fig. 1(a-1)) and a jet striking an infinite plate (fig. 1(a-4)). In these cases there are no surface sources. The plate merely acts as a reflector of the remaining sources, the ever present but inefficient volume sources (ref. 1). Data for the infinite plate (ref. 15) indicates that the plate has the same velocity power law as isolated jet noise; the sound power level is somewhat higher than that of the isolated jet because the plate modifies the turbulent flow (ref. 11). The data in reference 15 also show that the radiation pattern for the plate is the same as the pattern for the isolated jet, provided the impingement angle of the jet upon the plate is less than 60^o. The major effects of a finite jet on the radiation pattern for jet noise have already been incorporated into the theoretical pattern used herein for the volume source.

REFERENCES

1. Goldstein, M., Aeroacoustics, McGraw Hill, New York, 1976.

2. Amiet, R., "Acoustic Radiation from an Airfoil in a Turbulent Stream," Journal of Sound and Vibration, Vol. 41, Aug. 1975, pp. 407-420.

3. Olsen, W. A., "Noise Generated by Impingement of a Turbulent Jet on Isolated Airfoils of Varying Chord, Cylinders, and Other Flow Obstructions," AIAA Paper 76-504, July 1976.

4. Patterson, R., "Acoustic Radiation and Surface Pressure Characteristics of an Airfoil Due to Incident Turbulence," NASA CR 2733, 1976.

5. Olsen, W. A., Gutierrez, O. A., and Dorsch, R. G. "The Effect of Nozzle Inlet Shape, Lip Thickness, and Exit Shape and Size on Subsonic Jet Noise," AIAA Paper 73-187, Jan. 1973.

6. Olsen, W., and Friedman, R., "Jet Noise from Coaxial Nozzles Over a Wide Range of Geometric and Flow Parameters," AIAA Paper 74-43, Jan. 1974.

7. Hinze, J. O., Turbulence, McGraw-Hill Book Co., New York, 1959.

8. Laurence, J. C., "Intensity, Scale, and Spectra of Turbulence in Mixing Region of a Free Subsonic Jet," NASA TR-1292, 1956.

9. Fink, M. R. and Olsen, W. A., "Comparison of Predictions and Under-the-Wing EBF Noise Data," AIAA Paper 76-501, July 1976.

10. Olsen, W. A., Burns, R., and Groesbeck, D., "Flap Noise and Aerodynamic Results for Model QCSEE Over-the-Wing Configurations," AIAA Paper 77-23, Jan. 1977. (NASA TM X-73588, 1977.)

11. Boldman, D. R., and Brinich, P., "Mean Velocity, Turbulence Intensity, and Scale in a Subsonic Turbulent Jet Impinging Normal to a Large Flat Plate," NASA TP-1037, 1977.

12. Ffowcs Williams, J. and Hall, L. H., "Aerodynamic Sound Generation by Turbulent Flow in the Vicinity of a Scattering Half Plane," Journal of Fluid Mechanics, Vol. 40, Mar. 1970, pp. 657-670.

13. Becker, R. S., and Maus, J., Acoustic Source Location in the Secondary Mixing Region of a Jet-Blown Flap Using a Cross-Correlation Technique," AIAA Paper 77-1364, Oct. 1977.

14. Fink, M., "A Method for Calculating Externally Blown Flap Noise." NASA CR-2954, 1978.

15. Olsen, W. A., Miles, J. H., and Dorsch, R. G., "Noise Generated by Impingement of a Jet Upon a Large Flat Board," NASA TN D-7075, 1972.

16. McKinzie, D. J., Burns, R. J., and Wagner, J. M., "Noise Reduction Tests of Large-Scale-Model Externally Blown Flap Using Trailing-Edge Blowing and Partial Flap Slot Covering," NASA TM X-3379, 1976.

17. Hayden, R. E., "Sound Generation by Turbulent Wall Jet Flow Over a Trailing Edge," MS Thesis, Purdue Univ., 1970.

18. Goldstein, M., "Scattering and Distortion of the Unsteady Motion of Transversely Sheared Mean Flows," to be published.

19. "High Velocity Jet Noise Source Location and Reduction, Task 2-Theoretical Developments and Basic Experiments," U.S. Dept. Transportation, FAA-RD-76-79-II, 1978.

TABLE I. - ACOUSTIC CHARACTERISTICS[1] OF CONFIGURATIONS IN FIGURE 1

Ref. to fig. 1	Configuration	Experimentally determined velocity power law and radiation pattern (neglecting refraction)	Comments relative to theory
a-1	(a) Simple configurations: Jet noise (circular nozzle)	$I_p \propto d^2 V_n^8 (1 - 0.6\, V_n/C_o \cos\theta_e)^{-3}$ (max. I_p at $\theta_e = 0^o$) Reference 6 showed this pattern applies regardless of nozzle shape	Basic theory of ref. 1 verified
a-2	Small chord airfoil ($C/\ell_1 \leq 1$) Turbulence uniform spanwise and chordwise	$I_p \propto bC\, U_1^6 \sin^2\theta_e$ (max. at $\theta_e = 90^o$) Reference 3 shows effect of airfoil thickness, shape, angle of attack, etc.	Basic theory of ref. 1 also predicts spectra and level accurately. Source: fluctuating lift over the whole surface caused by turbulence.
a-3	Very large chord airfoil ($C/\ell_1 > 10$) Turbulence uniform spanwise and chordwise	$I_p \propto bC(\ell_1/C)\, U_1^5 \cos^2(\theta_e/2)$ (max. at $\theta_e = 0^o$), ref. 3.	Above small chord theory applies here at $\theta_e = 90^o$; it accurately predicts level and spectra, including wiggles. Source: fluctuating lift concentrated at leading edge due to compressibility.
	Intermediate chord airfoils ($1 < C/\ell_1 < 10$)	Result between above airfoil equations (ref. 3)	
	Above a-3 but no turbulence at leading edge	Same as a-3 but pattern is $\sin^2(\theta_e/2)$ (max. at $\theta_e = 180^o$) Result observed in ref. 17 at low velocity.	Source: above but now concentrated at trailing edge.
a-4	Infinite plate No significant turbulence at any edge	Approximately same as jet noise for impingement angles $< 60^o$ (ref. 15)	Theory shows that noise emission is like jet noise, with surface acting as a reflector; the surface also modifies the turbulent flow.
b-1	(b) Complex surfaces Three-flap UTW (approach flaps)	U_1^6 at all angles for low velocity; U_1^8 for small θ_e at high velocity, ref. 9	Only semi-empirical or empirical predictions exist. Mixed volume and surface sources.
b-2	Slotless wing UTW	Approaches U_1^8 for small θ_e and U_1^5 to U_1^6 for large θ_e, ref. 9.	
b-3	QCSEE OTW	Above but U_1^8 occurs over larger range of θ_e, ref. 10.	

[1]Subsonic flows, feedback tones neglected, acoustic data are free field and lossless.

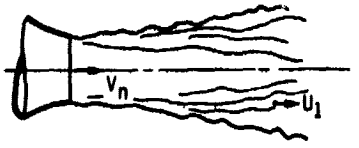

a-1. JET FROM CIRCULAR NOZZLE (VOLUME SOURCE)

a-2. SMALL CHORD AIRFOIL (SURFACE SOURCE)
HOMOGENEOUS TURBULENT FLOW

a-3. VERY LARGE CHORD AIRFOIL (SURFACE SOURCE)

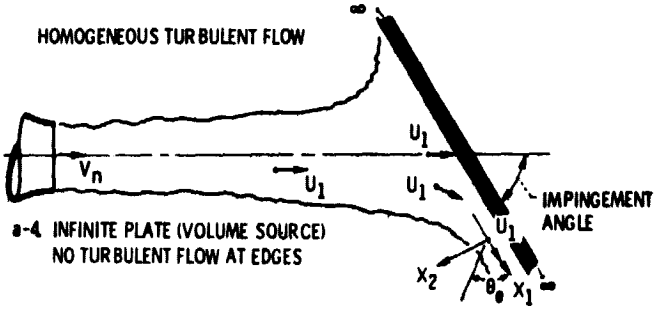

a-4. INFINITE PLATE (VOLUME SOURCE)
NO TURBULENT FLOW AT EDGES

(a) SIMPLE CONFIGURATIONS WITH SIMPLE FLOWS.

Figure 1. - Configurations studied.

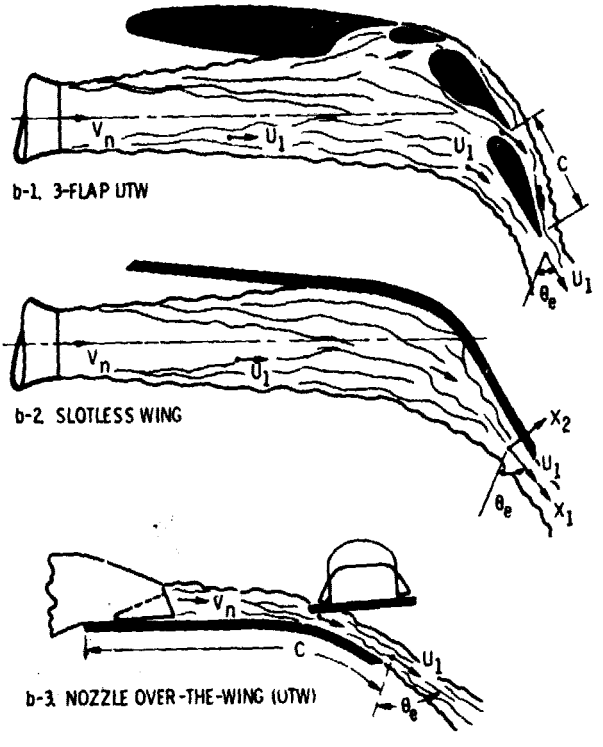

(b) COMPLEX SURFACES.

Figure 1. - Concluded.

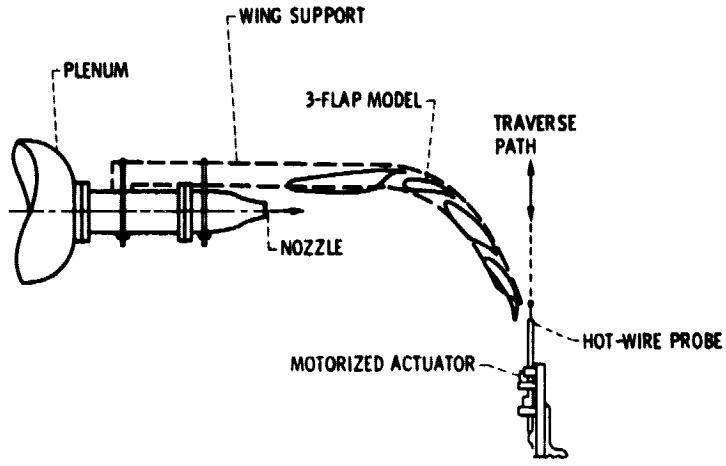

Figure 2 - Apparatus.

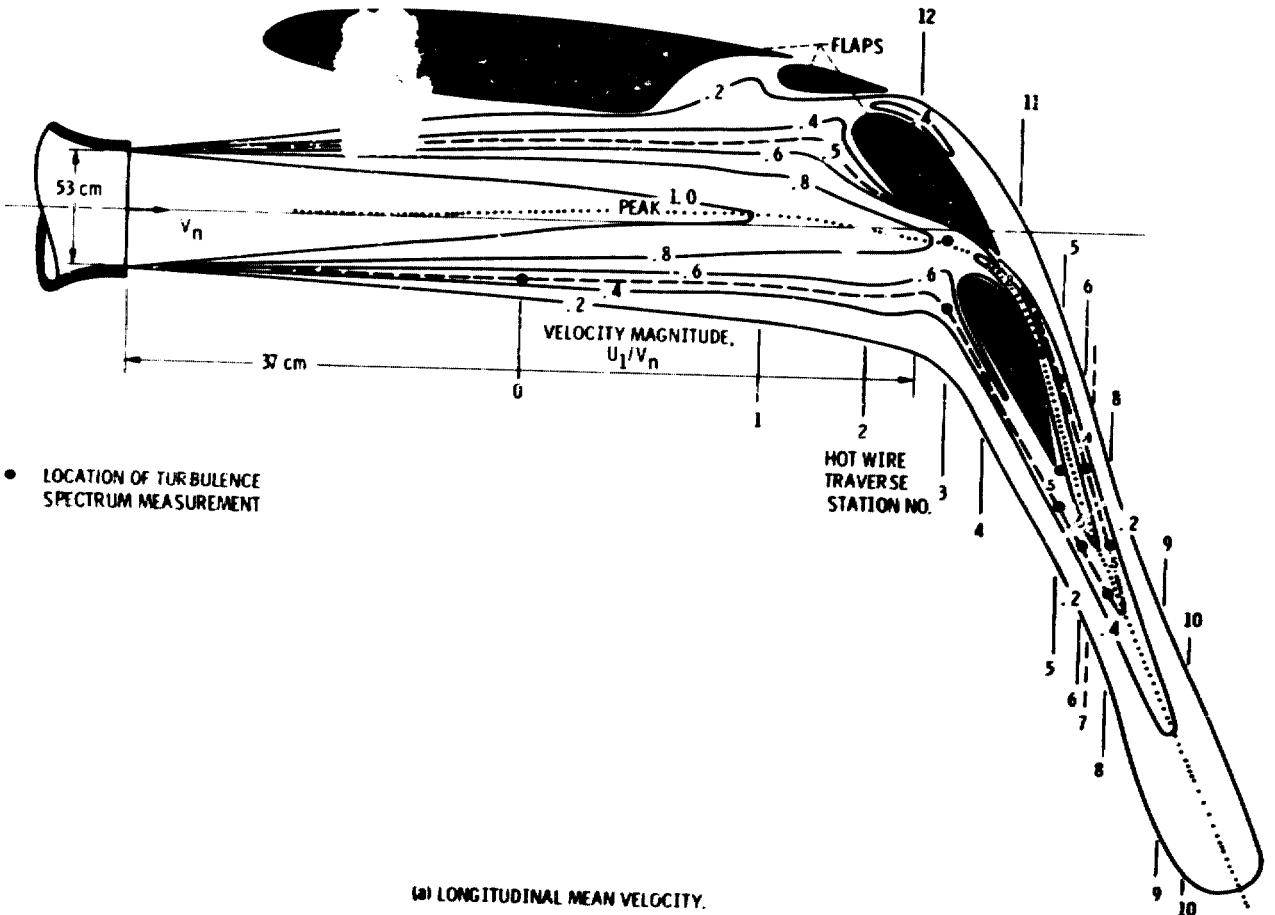

(a) LONGITUDINAL MEAN VELOCITY.

Figure 3. - Contour plots for 3-flap configuration. Hot wire traversed in midspan plane; drawing to scale; nozzle diameter, 5.3 cm; nozzle velocity, V_n, 90 m/sec.

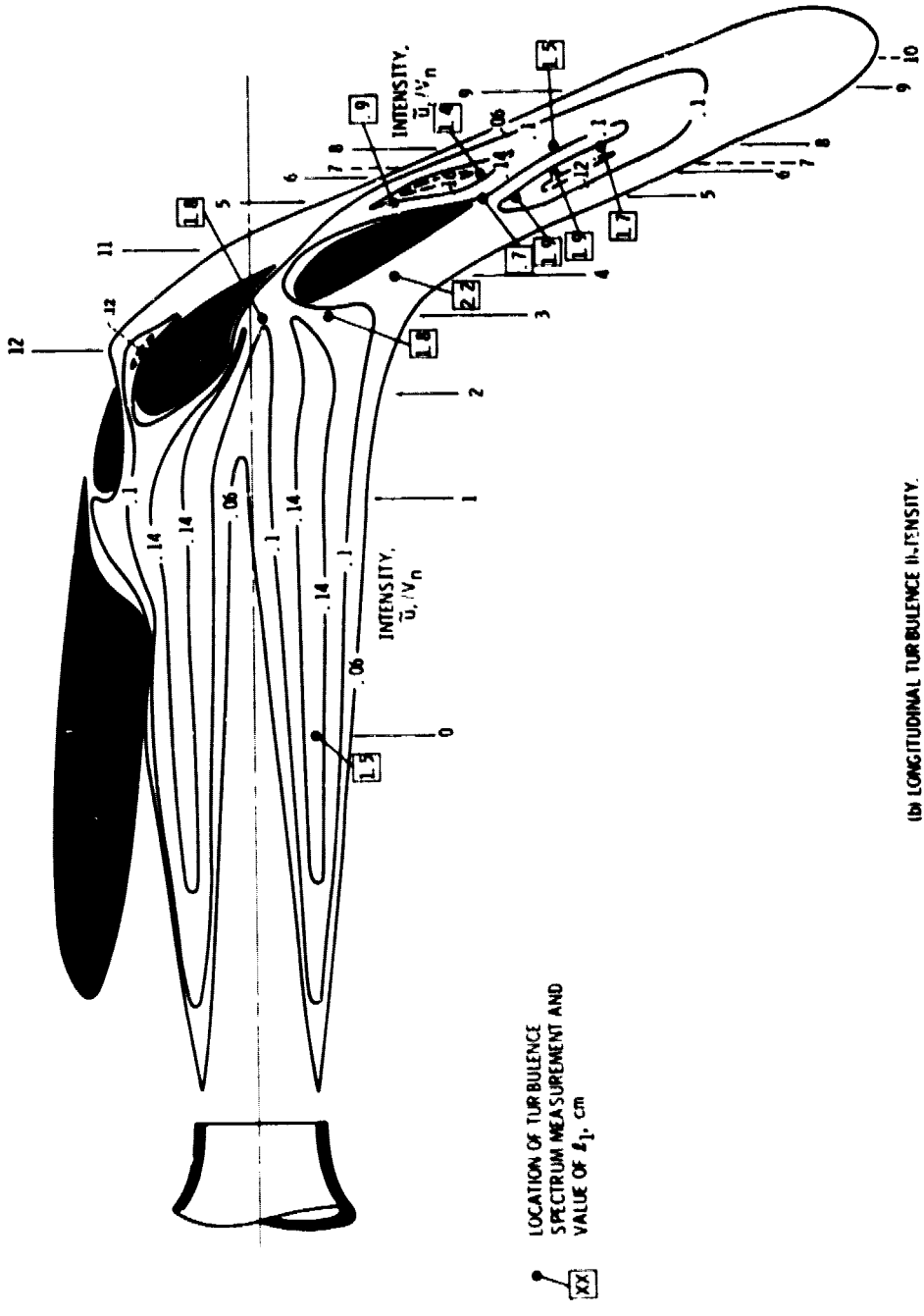

(b) LONGITUDINAL TURBULENCE INTENSITY.

Figure 3 - Concluded

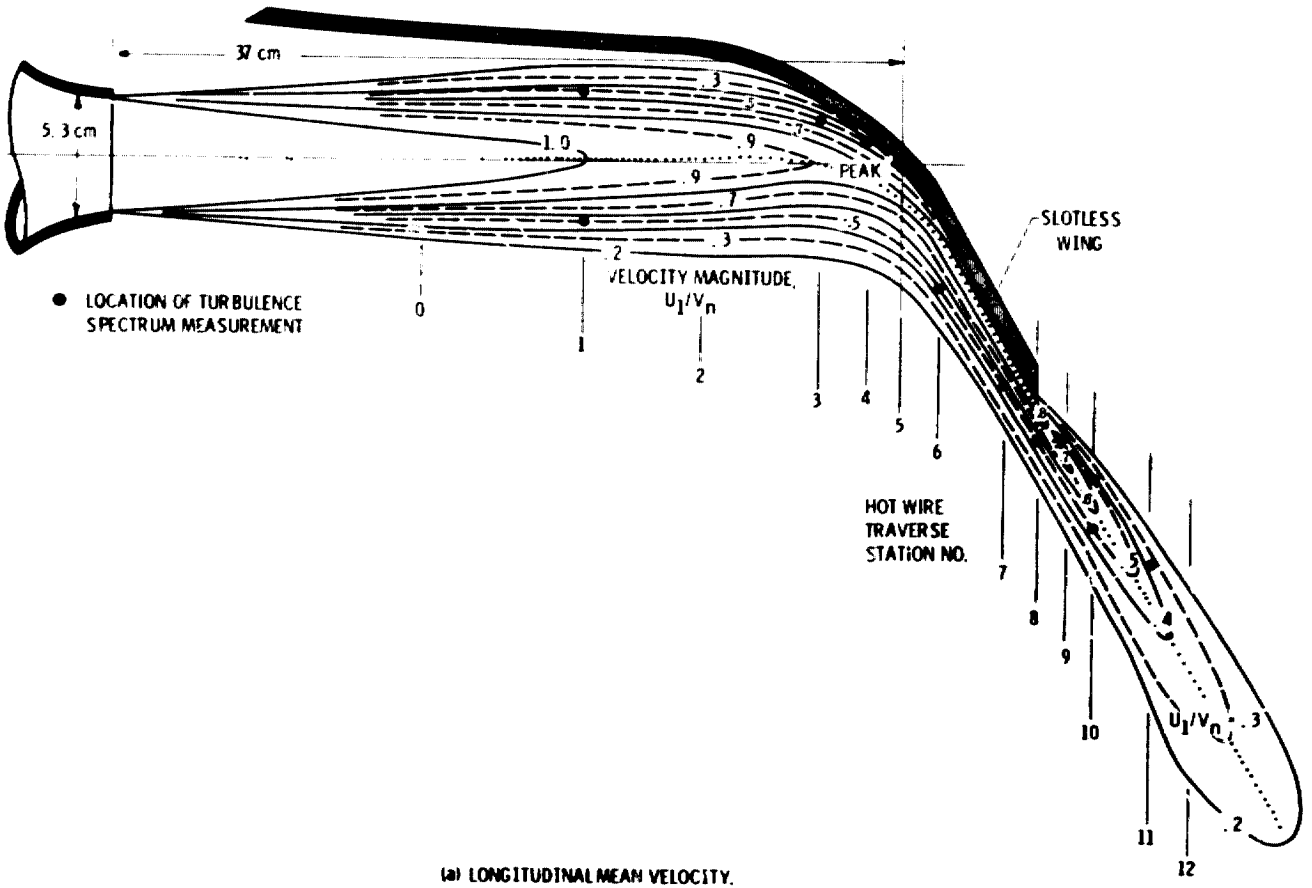

(a) LONGITUDINAL MEAN VELOCITY.

Figure 4. - Contour plots for slotless wing configuration. Hot wire traversed in midspan plane; nozzle diameter, 5.3 cm; nozzle velocity, V_n, 90 m/sec.

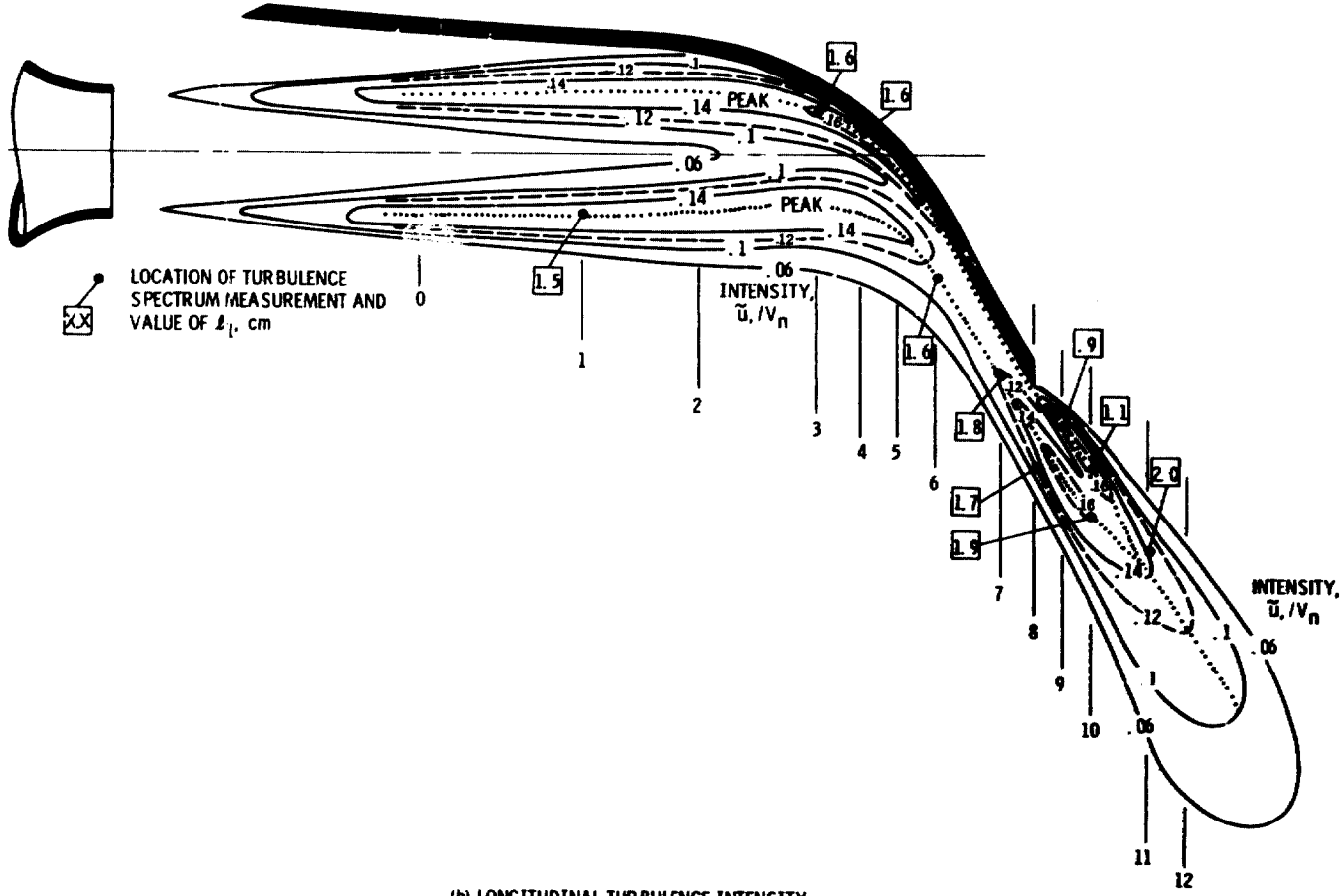

(b) LONGITUDINAL TURBULENCE INTENSITY.

Figure 4. - Concluded.

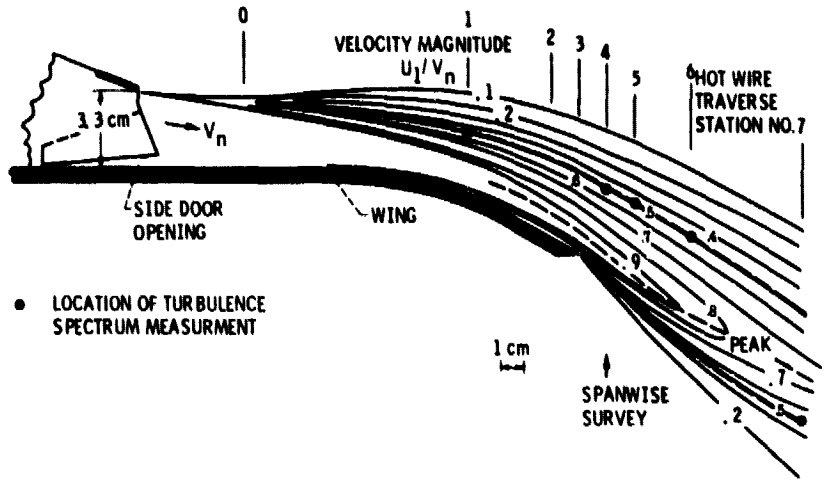

(a) LONGITUDINAL MEAN VELOCITY.

Figure 5. - Contour plots for OTW configuration. Hot wire traversed in midspan plane; drawing to scale; equivalent diameter, 5.3 cm nozzle velocity, V_n, 90 m/sec.

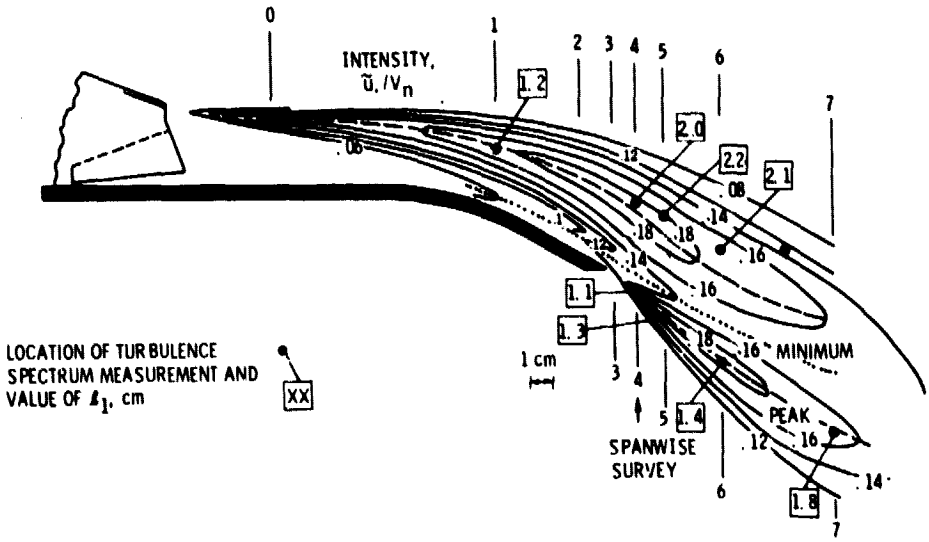

(b) LONGITUDINAL TURBULENCE INTENSITY.

Figure 5. - Concluded.

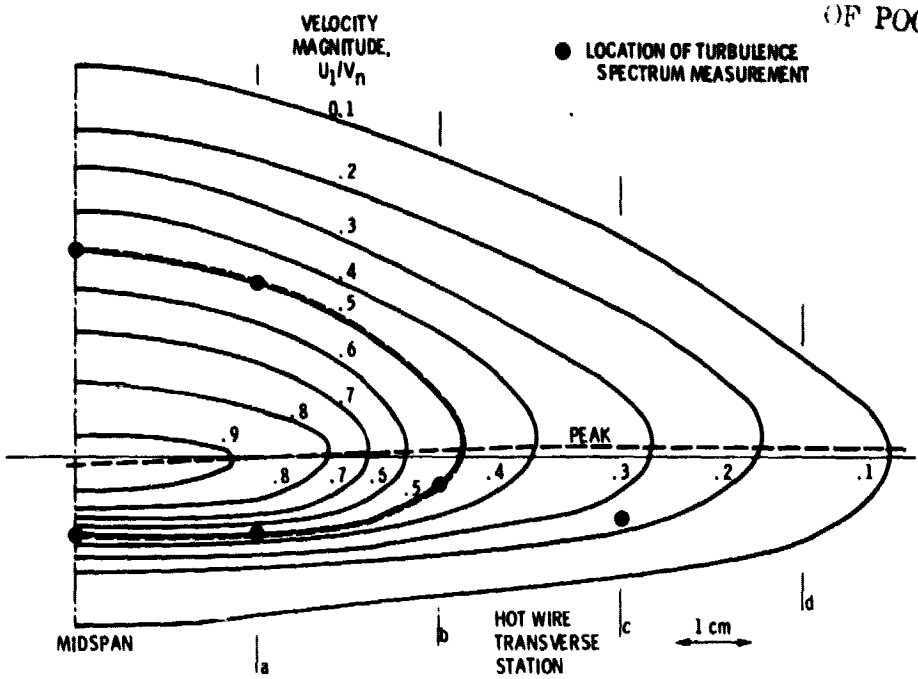

(a) LONGITUDINAL MEAN VELOCITY.

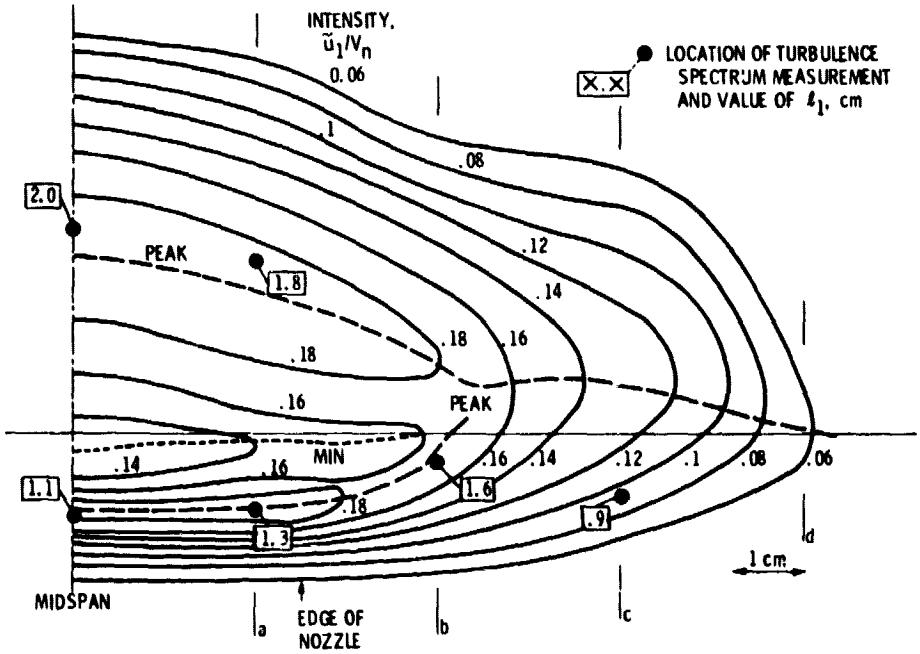

(b) LONGITUDINAL TURBULENCE INTENSITY.

Figure 6. - Spanwise contours in plane of traverse station no. 4 for OTW configuration. Equivalent diameter, 5.3 cm; nozzle velocity, V_n, 90 m/sec.

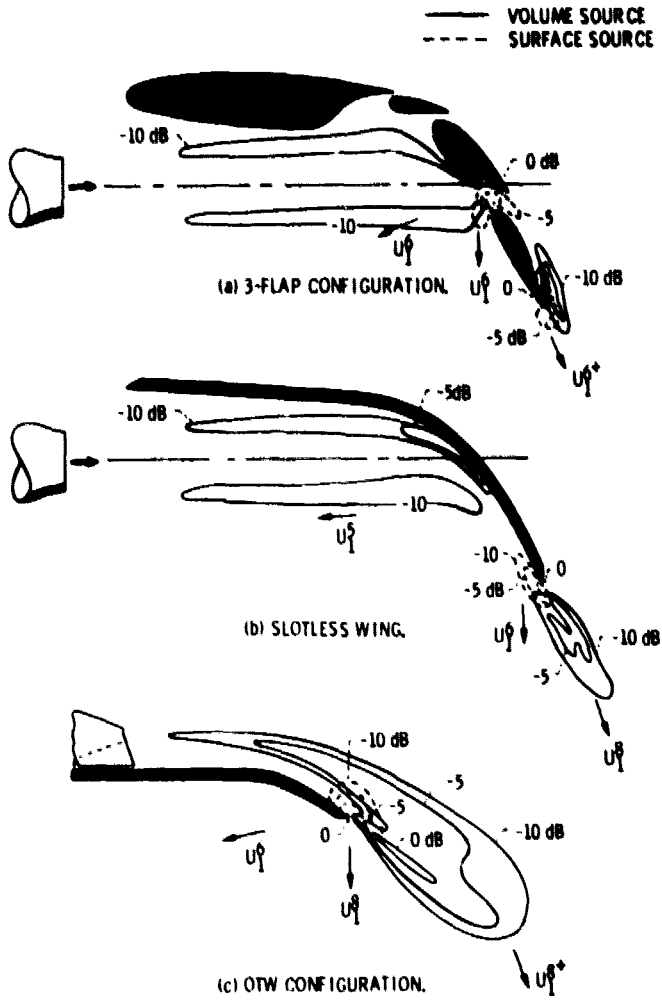

Figure 7. - Noise source locations. Peak intensities are calculated from equations 2 to 4 relative to a maximum intensity denoted as 0 dB: for volume sources used the maximum intensity for the three configurations; for surface source used the maximum intensity of each configuration.

1. Report No.	2. Government Accession No.	3. Recipient's Catalog No.
NASA TM-78944		

4. Title and Subtitle	5. Report Date
PRELIMINARY STUDY OF THE EFFECT OF THE TURBULENT FLOW FIELD AROUND COMPLEX SURFACES ON THEIR ACOUSTIC CHARACTERISTICS	6. Performing Organization Code

7. Author(s)	8. Performing Organization Report No.
W. A. Olsen and D. Boldman	E-9691
	10. Work Unit No.

9. Performing Organization Name and Address	11. Contract or Grant No.
National Aeronautics and Space Administration Lewis Research Center Cleveland, Ohio 44135	
	13. Type of Report and Period Covered
12. Sponsoring Agency Name and Address	Technical Memorandum
National Aeronautics and Space Administration Washington, D.C. 20546	14. Sponsoring Agency Code

15. Supplementary Notes

16. Abstract

Fundamental theories for noise generated by flow over surfaces exist for only a few simple configurations. The role of turbulence in noise generation by complex surfaces should be essentially the same as for simple configurations. Examination of simple-surface theories indicates that the spatial distributions of the mean velocity and turbulence properties (intensity, spectra, and integral scale length) are sufficient to define the noise emission. Measurements of these flow properties were made for a number of simple and complex (STOL aircraft blown flaps) surfaces. The configurations were selected because their acoustic characteristics (i.e. shape of radiation pattern and velocity power law) are quite different. The spatial distribution of the turbulent flow properties around the complex surfaces and approximate theory are used to locate and describe the noise sources, and to qualitatively explain the varied acoustic characteristics.

17. Key Words (Suggested by Author(s))	18. Distribution Statement
Aerodynamic noise Sources Noise	Unclassified - unlimited STAR Category 71

19. Security Classif. (of this report)	20. Security Classif. (of this page)	21. No. of Pages	22. Price*
Unclassified	Unclassified		

* For sale by the National Technical Information Service, Springfield, Virginia 22161